

Testing general relativity with binary black holes: a study on the sensitivity requirements for future space-based detectors

Tangchao Zhan,¹ Changfu Shi,¹ Shuo Sun,² and Jianwei Mei^{1,*}

¹*MOE Key Laboratory of TianQin Mission, TianQin Research Center for Gravitational Physics & School of Physics and Astronomy, Frontiers Science Center for TianQin, Gravitational Wave Research Center of CNSA, Sun Yat-sen University (Zhuhai Campus), Zhuhai 519082, China.*

²*School of Physical Science and Technology, Kunming University, Kunming 650214, China*

(Dated: March 18, 2026)

We study the sensitivity required for a future space-based detector to search for beyond general relativity effect in gravitational wave detection. To do this, we use the current design of TianQin, LISA, and μ Ares as starting points, and study how their key noise parameters should be improved to adequately detect some target signals, for which we choose a nonlinear ringdown mode, displacement memory, and a putative beyond general relativity signal, all from the merger of massive black hole binaries. We find that the required improvements are strongly dependent on the choice of the target signals and the population model of massive black hole binaries, and 4 – 9 orders of magnitude improvement will be needed in the most demanding detection scenarios.

I. INTRODUCTION

The breakthrough in Gravitational Wave (GW) detection [1] has given us the opportunity to probe the nature of gravity under conditions not possible before [2–11]. However, so far no violation of General Relativity (GR) has been identified in the detected GW signals [12–17]. This then leads to an intriguing question: If no Beyond GR Signal (BGRS) is found in any of the current GW detection missions, to what extent should one continue to improve the detection sensitivities? An answer to this question can help us better understand the prospect of searching for BGRS simply by improving the sensitivity of a detector and the level of technological improvement that will be needed for future missions. In this paper, we carry out a quantitative investigation of this problem.

To set meaningful detection goals, some target signals are needed, for which we consider two different scenarios for the search for BGRS.

- The first is to check if there is any inconsistency in the GR predicted signals. For this we consider two key predictions of GR in the merger of Massive Black Hole Binaries (MBHBs): the nonlinear $(2, 2, 0) \times (2, 2, 0)$ ringdown mode and the displacement memory. These signals contain the less explored nonlinear effects of GR and might have the opportunity to reveal the presence of BGRS.
- The second is to directly search for a putative BGRS. Unfortunately, so far no one is sure if or what BGRS can be detected with near-term detectors [10]. So we will try to motivate for one that is logically as obvious as possible. The BGRS we consider is motivated by an emergent gravity picture, where gravity is believed to be the effect of a hidden fluid [18, 19], and a black holes forms when the

underlying hidden fluid is forced into an extremely high density phase. We call this the Fluid Black Hole (FBH) model. In analogy to the violent collision of normal matter systems, during the merger of massive FBHBs, some mini black holes might be produced and, when the major remnant black hole is near extremal, may temporarily become satellite black holes orbiting the remnant black hole, forming Extreme Mass Ratio Inspirals (EMRIs). We call such systems induced Extreme Mass Ratio Inspirals (iEMRIs), whose detection would provide smoking gun evidence for new physics beyond GR.

We set the sensitivity requirements to be such that, given a chosen detector and a target signal, the detector should be able to detect the target signal from a significant portion of the events predicted by a chosen MBHB population model, such as Q3d, Q3nd and pop III [20, 21]. In this way, one can hope to confirm/exclude with good confidence if there is any sign of BGRS in the GW signals.

For reference detectors, we consider TianQin [22–24], LISA [25], and μ Ares [26]. These detectors are chosen because they represent space-based GW missions with a similar design but a vastly different choice of arm-lengths. Their sensitivity curves have a similar analytical form and are all controlled by two core noise parameters: the one way displacement measurement noise, $S_x^{1/2}$, for the inter-satellite laser interferometry, and the residual acceleration noise, $S_a^{1/2}$, of the test masses (i.e., inertial reference) along the sensitive directions. For each detector, we will keep its arm-length fixed and study how the noise parameters, $S_a^{1/2}$ and $S_x^{1/2}$, should be improved to achieve the desired sensitivity goals. In addition to the above, there are also other space-based GW detectors, such as Taiji [27] and DECIGO [28]. The results obtained in this study can also be of some reference value for them.

The most notable finding of the study is that the required improvements strongly depend on the actual pop-

* Corresponding author. Email: meijw@syzu.edu.cn

ulation model of MBHBs, with Q3d always leading to the least stringent requirements while pop III always leads to the most demanding requirements. Another notable feature is that, in the most demanding detection scenarios involving the putative iEMRI signal or the pop III population model, the required improvements in $S_a^{1/2}$ and $S_x^{1/2}$ can go up to 4–9 orders of magnitude, imposing a significant challenge for future development.

The paper is organized as follows. In section II, we introduce the main types of target signals and reference detectors to be used for this study. In section III, we describe the methods and present the main results of the paper. In section IV, we conclude with a brief summary.

II. THE TARGET SIGNALS AND REFERENCE DETECTORS

In this section, we briefly introduce the target signals that will be used for this study. These signals include the $(2, 2, 0) \times (2, 2, 0)$ ringdown mode, the displacement memory, and iEMRI. These signals are chosen because they are not only interesting targets for searching for new physics beyond GR, but are also relatively difficult to detect. We also introduce the three GW detectors that are used as possible starting points for future improvement.

A. The $(2, 2, 0) \times (2, 2, 0)$ ringdown mode

After the merger of a MBHB, the resulting compact remnant settles down to a stationary black hole by emitting GWs, which is the so called ringdown stage. The corresponding waveforms can be modeled by the sum of first-order Quasi-Normal Modes (QNMs), labeled by three indices (ℓ, m, n) [29]. When Signal-to-Noise Ratio (SNR) is large, nonlinear effects may also become important in the modeling of ringdown signals. The most relevant ones are the quadratic QNMs, which are solutions to the second-order perturbation theory [30] and are driven by quadratic combinations of the first-order QNMs [31], and so the quadratic QNMs are labeled by the corresponding first-order QNMs, $(\ell_1, m_1, n_1) \times (\ell_2, m_2, n_2)$. Understanding and detecting quadratic QNMs is not only an important direct test of the nonlinearities of GR, but is also important for the better modeling of the early ringdown signals.

Just like the first-order QNMs, the second-order ones are also damped sinusoids, whose oscillation frequencies, damping times, and amplitudes are related to the first-order ones through [31–33],

$$\begin{aligned} \omega_{(\ell_1, m_1, n_1)(\ell_2, m_2, n_2)} &= \omega_{\ell_1, m_1, n_1} + \omega_{\ell_2, m_2, n_2}, \\ \tau_{(\ell_1, m_1, n_1)(\ell_2, m_2, n_2)}^{-1} &= \tau_{\ell_1, m_1, n_1}^{-1} + \tau_{\ell_2, m_2, n_2}^{-1}, \\ A_{(\ell_1, m_1, n_1)(\ell_2, m_2, n_2)} &= \mu_{(\ell_1, m_1, n_1)(\ell_2, m_2, n_2)} \\ &\quad \times A_{\ell_1, m_1, n_1} A_{\ell_2, m_2, n_2}. \end{aligned} \quad (1)$$

There are two methods to determine the ratio factor $\mu_{(\ell_1, m_1, n_1)(\ell_2, m_2, n_2)}$. The first involves directly fitting Eq. (1) to existing numerical relativity data [33–35], and the second involves solving second-order perturbation equations using numerical methods [36–39]. The results of both methods are consistent with each other, and it has been found that $\mu_{(\ell_1, m_1, n_1)(\ell_2, m_2, n_2)}$ only depends on the properties of the remnant black hole, especially its spin [37, 38]. In this paper, we will focus on the detection of the $(2, 2, 0) \times (2, 2, 0)$ mode, for which [35]

$$\mu_{(2,2,0)(2,2,0)} = 0.1637. \quad (2)$$

So far, the evidence for quadratic QNMs in GW signals is still very limited. In GW250114, the signal with the highest SNR (nearly 80) to date, clear evidence of higher-order ringdown modes and overtones has been established [40, 41]. It has been pointed out that including the second-order $(2, 2, 0) \times (2, 2, 0)$ mode can better explain the ringdown signal of GW250114, and $(2, 2, 0) \times (2, 2, 0)$ fits the data better than the $(4, 4, 0)$ mode [42]. By including inspiral and merger data, a Bayes factor of 74 has been found to support the existence of the $(2, 2, 0) \times (2, 2, 0)$ mode in the ringdown data in [43]. For future space-based GW detectors, TianQin and LISA can detect 2–15 and 6–50 events, respectively, that contain a detectable contribution from the $(2, 2, 0) \times (2, 2, 0)$ mode, with roughly half of which are resolvable despite mixing from other modes [44].

B. The displacement memory

After the passage of GW, the relative separation between two objects in spacetime experiences a permanent displacement, this effect is known as the GW memory effect [45–47]. In an asymptotically flat spacetime, the memory effect has been shown to closely relate to various Bondi-Sachs-Metzner (BMS) transformations [48–51]. Meanwhile, the memory effect has been shown to be closely related to Weinberg’s soft graviton theorem [52], which leads to the so-called infrared triangle, which connects the memory effect, asymptotic symmetries, and soft theorems [53]. In addition to GR, memory effects have also been studied in other modified theories of gravity, such as Brans–Dicke theory [54, 55], Scalar-Tensor theory [56], Chern–Simons theory [57, 58] and Einstein–Æther theory [59]. Therefore, the detection of the GW memory effect is of great importance, such as testing GR in the nonlinear regime [46, 56], improving the precision of parameter estimation for GW signals [60, 61], and helping to study the asymptotic symmetry of spacetime [62].

The BMS symmetry allows a neat classification of the different types of memory effect: displacement memory, spin memory, and center-of-mass memory, which are related in one to one correspondence to supertranslation, superrotation, and superboost, respectively. Among the three, the displacement memory is always the strongest and will be chosen as a detection target for this paper.

The study of the detectability of the GW memory effect started in the 1980s [63]. After the detection of GW150914, existing ground-based detectors have been found to remain insufficient for direct observation of the memory effect, neither from a single event [64] nor from the joint analysis of multiple events from GWTC-1, GWTC-2, and GWTC-3 [65–67]. However, it has been found that next-generation detectors, such as the Cosmic Explorer [68] and the Einstein Telescope [69], may have the potential to directly detect the GW memory effect [62]. The prospect of detecting the memory effect with a space-based GW detector has been analyzed for TianQin in [61, 70] and LISA in [71, 72]. Both detectors have the opportunity to detect some MBHB signals that contain a detectable memory effect. The possibility of detecting the memory effect using pulsar timing arrays has been explored in [73–78]. Based on approximately 12.5 years of NANOGrav data, a Bayes factor of 2.8 has been obtained for the memory effect [79].

C. iEMRI

There are largely two different ways to model and theorize gravity using only particles.¹ The first is to assume that gravity is mediated by a fundamental force carrier, usually a boson called graviton. In this case, gravity is a fundamental interaction of nature, and the spacetime metric is treated as the fundamental gravitational field, but the quantization of which has faced a lot of difficulties. The second is to assume that gravity is caused by the coupling of matter to some hidden condensed matter system, usually made of interacting fermions. In this case, gravity is emergent [80–85], and the spacetime metric is expected to be determined by either the properties of the hidden condensed matter system itself or its phonon-like excitations. At the macroscopic scale, one expects that an interacting particle system can be treated as a fluid in the general sense, and so gravity is also expected to be determined by the properties of a fluid, which we call hidden fluid.

A quantitative relation between spacetime metric and hidden fluid has been explored in [18, 19] and some intriguing results have been found. For example, the density of hidden fluid underlying a Schwarzschild black hole is given by

$$\varrho(r) = \frac{\varrho_0}{1 - 2M/r}, \quad (3)$$

where M is the mass of the black hole, r is the Boyer-Lindquist radial coordinate, ϱ_0 is the average density of hidden fluid at spatial infinity. The divergence of the density at the black hole horizon implies that some new

physics must come into play before the horizon is reached. If an analogy to normal matter can be made, then hidden fluid is expected to be forced into an incompressible phase, whose density cannot be further increased, when the density of hidden fluid reaches a high critical value $\varrho_{\text{cri}} = \varrho_0/(1 - 2M/r_{\text{cri}})$. In this case, the density of hidden fluid is governed by (3) outside a Schwarzschild black hole, while that inside the black hole becomes a constant.

Motivated by the above results, we consider the following FBH model, illustrated for a Schwarzschild black hole in Fig. 1. In this model, the FBH corresponds to a region of spacetime where hidden fluid is in the incompressible phase, with $\varrho \sim \varrho_{\text{cri}}$. The GR predicted event horizon is inside the FBH, $r_{\text{H}} < r_{\text{cri}}$, and is no longer relevant. Outside the FBH, hidden fluid is in the compressible phase and $\varrho(r)$ is a monotonically decreasing function of r , with $\varrho(r_{\text{cri}}) = \varrho_{\text{cri}}$ and $\varrho(\infty) = \varrho_0$. The exact detail of $\varrho(r)$ depends on the specific relation between spacetime metric and hidden fluid being explored, with (3) being a specific example.

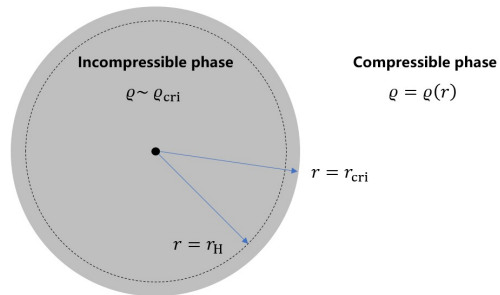


FIG. 1. An illustration of the FBH model for a Schwarzschild black hole.

Due to the composite nature of FBHs, some behavior similar to normal matter systems might be expected. For example, during the violent encounter of two FBHs, small segments of highly dense hidden fluid, which are effectively mini black holes, might be produced and ejected out of the collision region. When the major remnant black hole is near extremal, there is the chance for an ejected mini black hole to get enough initial angular velocity to temporarily become a satellite black hole orbiting the remnant black hole. In this case, the pair becomes an iEMRI. The mini black holes are expected to fly only for a short time and then return to the major remnant black holes. So, iEMRIs are expected to be short lived.

A detection of the iEMRI signal will provide the smoking gun evidence for new physics beyond GR. This is because in GR the second law of thermodynamics forbids a black hole from splitting into two or more black holes (see, e.g. [86] and references therein). As a result, the close encounter of two black holes always produces only one black hole in GR, even during a relativistic black hole collision [87–94].

¹ We do not consider theories that involve extended fundamental objects, such as strings or branes.

D. The reference detectors

We use the following three detectors as reference detectors for this study.

- TianQin consists of three geocentric satellites that form a nearly equilateral triangle with an arm length $L_{\text{TQ}} \approx 1.7 \times 10^8$ m. The sensitivity band of TianQin is assumed to be $10^{-4} - 1$ Hz [22–24].
- LISA consists of three spacecraft that form a nearly equilateral triangle with an arm length $L_{\text{LISA}} \approx 2.5 \times 10^9$ m. It will operate in an Earth-like heliocentric orbit, approximately 20° apart from Earth. The LISA sensitivity band is assumed to be $2 \times 10^{-5} - 1$ Hz [25].

- μAres is a future $\mu\text{-Hz}$ space-based detector consists of two equilateral triangle constellations with an arm length of $L_{\mu\text{Ares}} = 4.3 \times 10^{11}$ m. The sensitivity band of μAres is assumed to be $10^{-7} - 1$ Hz [26]. In this study, we only consider one of the two constellations of μAres .

These detectors are chosen because they have a good prospect of detecting MBHB signals, their sensitivities share the same set of key noise parameters, and their arm lengths take a hierarchy of different values. These are helpful for making a meaningful comparison.

The sky-averaged sensitivities of TianQin and LISA are given by:

$$S_n^{\text{TQ}}(f) = \frac{10}{3L_{\text{TQ}}^2} \left[S_x^{\text{TQ}} + \frac{4S_a^{\text{TQ}}}{(2\pi f)^4} \left(1 + \frac{10^{-4}\text{Hz}}{f} \right) \right] \times \left[1 + 0.6 \left(\frac{f}{f_*^{\text{TQ}}} \right)^2 \right], \quad (4)$$

$$S_n^{\text{LISA}}(f) = \frac{10}{3L_{\text{LISA}}^2} \left\{ S_x^{\text{LISA}}(f) + \frac{S_a^{\text{LISA}}(f)}{(2\pi f)^4} \left[1 + \cos^2 \left(\frac{f}{f_*^{\text{LISA}}} \right) \right] \right\} \times \left[1 + \frac{6}{10} \left(\frac{f}{f_*^{\text{LISA}}} \right)^2 \right]. \quad (5)$$

Here, $f_*^{\text{TQ}} = c/2\pi L_{\text{TQ}} \approx 0.28\text{Hz}$ is the transfer frequency of TianQin, $(S_x^{\text{TQ}})^{1/2} = 1 \times 10^{-12}\text{m/Hz}^{1/2}$ is the noise of the one-way displacement measurement, and $(S_a^{\text{TQ}})^{1/2} = 1 \times 10^{-15}\text{m/s}^2/\text{Hz}^{1/2}$ is the residual acceleration noise [22–24]. Similarly, $f_*^{\text{LISA}} = 1/(2\pi L_{\text{LISA}}) \approx 0.02\text{Hz}$ is the transfer frequency of LISA, and

$$\begin{aligned} S_x^{\text{LISA}}(f) &= S_x^{\text{LISA}} \left[1 + \left(\frac{2 \times 10^{-3}\text{Hz}}{f} \right)^4 \right], \\ S_a^{\text{LISA}}(f) &= S_a^{\text{LISA}} \left[1 + \left(\frac{4 \times 10^{-4}\text{Hz}}{f} \right)^2 \right] \\ &\quad \times \left[1 + \left(\frac{f}{8 \times 10^{-3}\text{Hz}} \right)^4 \right], \end{aligned} \quad (6)$$

where $(S_x^{\text{LISA}})^{1/2} = 1.5 \times 10^{-11}\text{m/Hz}^{1/2}$ and $(S_a^{\text{LISA}})^{1/2} = 3 \times 10^{-15}\text{m/s}^2/\text{Hz}^{1/2}$ [25, 95].

The analytical formula for the sensitivity of μAres is currently unavailable. We assume that it has the same structure as (5), replacing LISA everywhere with μAres , and fit it to Fig. 1 of [26] to obtain the following:

$$\begin{aligned} S_x^{\mu\text{Ares}}(f) &= S_x^{\mu\text{Ares}} \left[1 + \left(\frac{1 \times 10^{-3}\text{Hz}}{f} \right)^4 \right], \\ S_a^{\mu\text{Ares}}(f) &= S_a^{\mu\text{Ares}} \left[1 + \left(\frac{4 \times 10^{-6}\text{Hz}}{f} \right)^2 \right] \\ &\quad \times \left[1 + \left(\frac{f}{8 \times 10^{-3}\text{Hz}} \right)^4 \right], \end{aligned} \quad (7)$$

where $(S_x^{\mu\text{Ares}})^{1/2} = 3.5 \times 10^{-11}\text{m/Hz}^{1/2}$ and

$$(S_a^{\mu\text{Ares}})^{1/2} = 2 \times 10^{-15}\text{m/s}^2/\text{Hz}^{1/2}.$$

A comparison of the sensitivities of the three reference detectors can be found in Fig. 3.

III. METHOD AND RESULTS

In addition to the three types of target signals and three reference detectors, we also consider three population models of merging MBHBs: Q3d, Q3nd and pop III [20, 21]. For each population model, we have 10 independent samples, each containing a different number of sources. We combine them to get a super-sample for each population model, containing 405, 6122 and 8735 sources in total for Q3d, Q3nd and pop III, respectively. In this section, all the population-based plots are made using the super-samples. So, if one wants to estimate some detection number by counting individual sources in a plot, one should divide the result by 10.

Each combination of a source, a target signal, and a reference detector is treated as a detection problem. For each detection problem, we want to find the optimal values of $(S_a^{1/2}, S_x^{1/2})$, which not only need to allow the target signal to be detected with enough SNR but also need to place the least demanding requirement on the development of technology. To calculate SNR, we use

$$\rho = \sqrt{\langle h|h \rangle}, \quad (8)$$

where h is the waveform of the target signal. The inner

product is defined as:

$$(a(f)|b(f)) = 2 \int_{f_{\text{low}}}^{f_{\text{high}}} \frac{a^*(f)b(f) + a(f)b^*(f)}{S_n(f)} df, \quad (9)$$

where $S_n(f)$ is the sky-averaged sensitivity of the detector under consideration. Throughout the study, we fix the detection threshold as $\rho_{\text{th}} = 8$. This threshold has been used in some previous studies [44, 61], but its exact value is not expected to bring an order of magnitude difference to the main conclusions of this paper.

For each detection problem, SNR becomes a function of the noise parameters $\rho = \rho(S_a^{1/2}, S_x^{1/2})$, and this function has a remarkable feature as illustrated in Fig. 2. To understand the behavior, note $\rho(S_a^{1/2}, 0) = 8$ and $\rho(0, S_x^{1/2}) = 8$ lead to constant solutions of $S_a^{1/2}$ and $S_x^{1/2}$, respectively, so the blue curve corresponding to $\rho(S_a^{1/2}, S_x^{1/2}) = 8$ is nearly horizontal when $S_x^{1/2} \rightarrow 0$ and nearly vertical when $S_a^{1/2} \rightarrow 0$. Thus, a horizontal line and a vertical line (the dashed ones) can be drawn that are tangential to the blue curve and meet at the point O' . In the region where the blue curve turns from horizontal to vertical, the contributions of $S_a^{1/2}$ and $S_x^{1/2}$ are comparable to each other. This is where we pick the optimal values for $(S_a^{1/2}, S_x^{1/2})$ for each detection problem. In practice, one would compare the technical difficulties in improving $S_a^{1/2}$ and $S_x^{1/2}$, and then decide which value to choose. For this study, however, we will simply draw a line of slope 1² that starts from the point O' and intersects the blue curve at the point O , and then take the latter to be the optimal choice of $(S_a^{1/2}, S_x^{1/2})$.

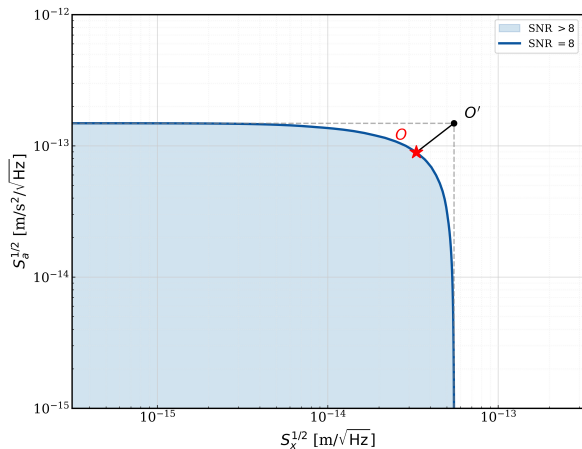


FIG. 2. The allowed values of $(S_a^{1/2}, S_x^{1/2})$ for a detection problem. In the plot, the target signal is the $(2, 2, 0) \times (2, 2, 0)$ ringdown mode, the reference detector is TianQin, and the injected source parameters are: $m_1 = 3 \times 10^4 M_\odot$, $m_2 = 2 \times 10^4 M_\odot$, $z = 1$, $\iota = \pi/4$, and $\phi = 0$. See main text for more explanation.

² For this we always assume a log-log plot and take the units of axes to be same as in Fig. 2.

For a given target signal and a given reference detector, each source determines an optimal choice of $(S_a^{1/2}, S_x^{1/2})$, corresponding to a point in the parameter space of $(S_a^{1/2}, S_x^{1/2})$. The results for all sources in a super-sample then determine a distribution. The results are plotted in Figs. 4-6. Some source selection has been performed when making the plots. This is necessary because some of the target signals impose additional restrictions.

- **$(2, 2, 0) \times (2, 2, 0)$ mode:** All sources are used.
- **Displacement memory:** Only sources with a mass ratio $q \in [1, 25]$ are used. Our calculation of the memory waveform depends on IMRPhenomXHM [96–98], which has been calibrated with numerical relativity within $q \in [1, 18]$ but is believed to have a reasonable accuracy outside of this range [96]. To transform the memory waveform from the time domain to the frequency domain, we use the method of [99].
- **iEMRI:** We only consider sources in which the remnant black hole is near extremal, and only consider the radiation from the last cycle before plunge. The corresponding waveform is generated with `kerrgeodesic_gw` [100], which supports spins 0.9 and 0.95 for the central black hole. For these reasons, we only consider sources with final spins in the range $[0.875, 0.975]$. Those in the range $[0.875, 0.925]$ are approximated to have spin 0.9, and those in the range $[0.925, 0.975]$ are approximated to have spin 0.95. We also assume that the mass of the mini black hole is always 10^{-6} times that of the central black hole.

For each distribution, we define its center to be at the center-of-mass location, assuming log-log scale and equal weight for all the sources. See the last rows of Figs. 4-6. Given a target signal, a reference detector and a population model, the required improvement in technology is characterized by the difference between the current location of the detector in the parameter space of $(S_a^{1/2}, S_x^{1/2})$ and the center of the corresponding distribution.

Fig. 4 contains the results for TianQin. There are a few obvious features.

- To detect the $(2, 2, 0) \times (2, 2, 0)$ ringdown mode, it will be more effective if S_x can be significantly improved. The improvement in $S_x^{1/2}$ should be about 2, 3 and 6 orders of magnitude if the population model is Q3d, Q3nd and pop III, respectively.
- To detect displacement memory, it will be more effective if S_a can be significantly improved. The improvement in $S_a^{1/2}$ should be about 2, 3 and 4 orders of magnitude if the population model is Q3d, Q3nd and pop III, respectively.
- To detect iEMRI, both S_a and S_x need to be significantly improved. The improvement in $S_a^{1/2}$ should

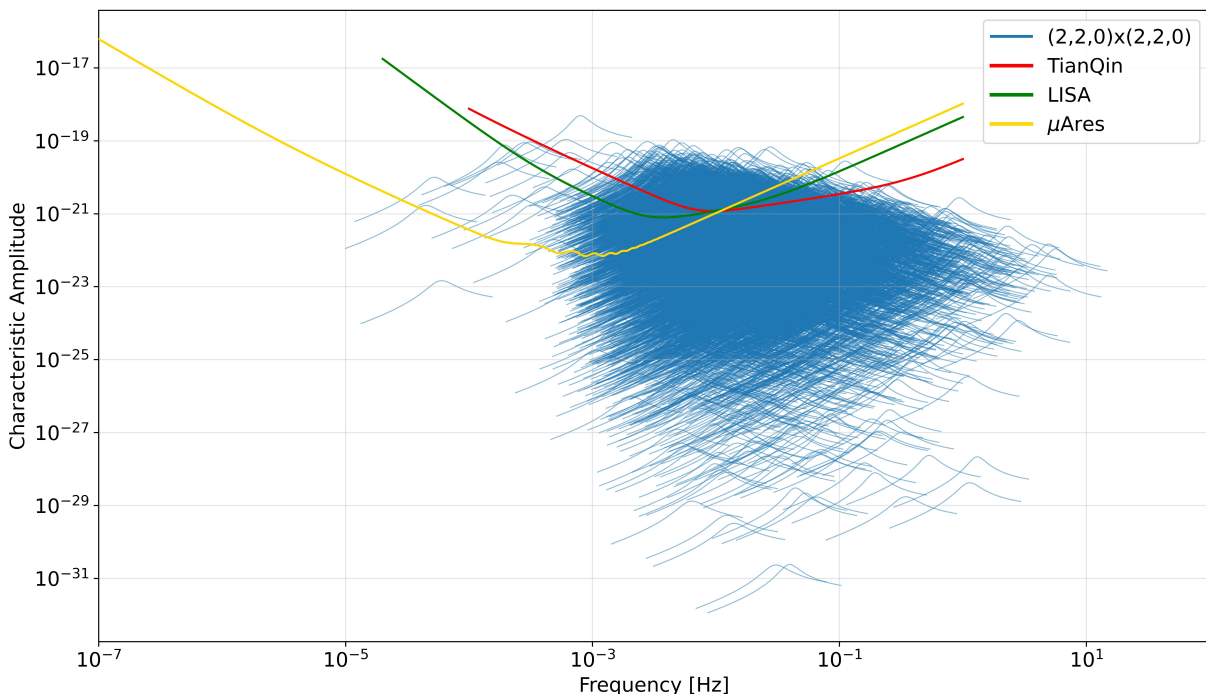


FIG. 3. Signal of the $(2, 2, 0) \times (2, 2, 0)$ ringdown mode for all sources in the Q3nd super-sample. The sensitivity curves of the three reference detectors are also shown as a comparison.

be about 4 orders of magnitude for all population models, while the improvement in $S_x^{1/2}$ should be about 4, 5 and 7 orders of magnitude if the population model is Q3d, Q3nd and pop III, respectively.

- The requirements from pop III are always the most stringent, typically of 3-7 orders of magnitude, while those from Q3d are always the least demanding, typically of 0-4 orders of magnitude.

In the detection of the $(2, 2, 0) \times (2, 2, 0)$ ringdown mode, some of the distributions show clear straight edges. In particular, the distribution of Q3nd (first plot in the second row of Fig. 4) is bounded both from the upper-left edge and from the lower-right edge. To understand this, in Fig. 3 we plot all the waveforms of the $(2, 2, 0) \times (2, 2, 0)$ ringdown mode for all sources in the Q3nd super-sample. The waveforms of the lightest sources are partially outside the sensitivity band of TianQin, which is $10^{-4} - 1$ Hz. The part of their waveforms remaining in the band become nearly identical to each other, differing only by a scaling of their magnitudes. This causes them to be distributed in the same line in the parameter space of $(S_a^{1/2}, S_x^{1/2})$, forming the upper-left edge. For the heavy sources, one can see in Fig. 3 that there is a significant amount of low frequency signals distributed near 10^{-3} Hz. These signals also have nearly identical waveforms that differ only by scaling of their magnitudes. This also causes them to be distributed along the same line, forming the lower-right edge.

Compared to Fig. 4, the most significant feature of

Fig. 5 and Fig. 6, corresponding to LISA and μ Ares, respectively, is that most of the sources are distributed very close to a narrow line. To understand this, note that most signals in Fig. 3 are distributed in frequencies higher than 10^{-3} Hz. For the majority of them, (6) can be approximated as

$$S_x^{\text{LISA}}(f) \approx S_x^{\text{LISA}},$$

$$S_a^{\text{LISA}}(f) \approx S_a^{\text{LISA}} \left(\frac{f}{8 \times 10^{-3} \text{ Hz}} \right)^4. \quad (10)$$

Consequently, the most significant piece of frequency dependence cancels out in (5) through the combination $S_a^{\text{LISA}}(f)/(2\pi f)^4$, and S_x and S_a contribute to (5) through a nearly frequency-independent combination, resulting in a constant ratio between their optimal values. Only for a small number of very massive sources, which have a significant contribution from frequencies near 10^{-3} Hz, can one observe some deviation from the narrow line distribution. The same is true for μ Ares.

Another obvious feature is that, just like for TianQin, Q3d always places the least stringent requirements on technology improvement, typically no higher than 4 orders of magnitude, while those from pop III are typically 3 – 6 orders more demanding.

Some of the numerical results are summarized in Tables I-III, where 220Q stands for $(2, 2, 0) \times (2, 2, 0)$ and we have defined

$$q_a = \frac{S_a^{\text{opt}}}{S_a^{\text{det}}}, \quad q_x = \frac{S_x^{\text{opt}}}{S_x^{\text{det}}}. \quad (11)$$

Here, S_a^{opt} and S_x^{opt} represent the center values of a given distribution, and S_a^{det} and S_x^{det} represent the current values of the corresponding detector.

TABLE I. The required improvement in the key noise parameters of TianQin

TianQin		Q3d	Q3nd	pop III
220Q	q_a	3.05	3.08×10^{-1}	8.45×10^{-3}
	q_x	1.75×10^{-2}	1.25×10^{-3}	1.40×10^{-6}
Memory	q_a	2.71×10^{-2}	4.94×10^{-3}	1.81×10^{-4}
	q_x	5.69	4.48×10^{-1}	8.93×10^{-4}
iEMRI	q_a	5.01×10^{-4}	3.38×10^{-4}	6.04×10^{-4}
	q_x	2.69×10^{-4}	6.23×10^{-5}	1.04×10^{-7}

TABLE II. The required improvement in the key noise parameters of LISA

LISA		Q3d	Q3nd	pop III
220Q	q_a	4.78×10^{-1}	2.65×10^{-2}	4.58×10^{-6}
	q_x	6.63×10^{-2}	3.19×10^{-3}	4.64×10^{-7}
Memory	q_a	3.21×10^{-1}	6.59×10^{-2}	1.46×10^{-3}
	q_x	4.81×10^{-1}	7.06×10^{-2}	6.25×10^{-4}
iEMRI	q_a	9.93×10^{-4}	3.08×10^{-4}	1.09×10^{-7}
	q_x	2.37×10^{-4}	4.92×10^{-5}	1.05×10^{-8}

TABLE III. The required improvement in the key noise parameters of μ Ares

μ Ares		Q3d	Q3nd	pop III
220Q	q_a	1.54	6.56×10^{-2}	7.17×10^{-6}
	q_x	9.32×10^{-2}	3.68×10^{-3}	5.30×10^{-7}
Memory	q_a	19.6	2.32	1.68×10^{-2}
	q_x	27.1	2.84	1.51×10^{-2}
iEMRI	q_a	5.97×10^{-3}	1.22×10^{-3}	1.68×10^{-7}
	q_x	5.08×10^{-4}	6.41×10^{-5}	4.63×10^{-9}

IV. SUMMARY

In this paper, we investigate how much improvement in sensitivity will be needed to search for a possible BGRS with future space-based GW detectors. The main purpose is to obtain a quantitative understanding of the

prospect of searching for BGRS simply by improving the sensitivity of a detector.

We use TianQin, LISA and μ Ares as reference detectors and study how their key noise parameters, S_a and S_x , should be improved to meet a set of detection goals, for which we use the $(2, 2, 0) \times (2, 2, 0)$ ringdown mode, displacement memory and iEMRI as target signals, and use Q3d, Q3nd and pop III as the MBHB population models. For a given type of target signal, a reference detector, and a population model, we determine how the noise parameters should be improved so that the target signal can be detected from a significant portion of the sources predicted by the population model. In this way, one can hope to confirm/exclude with good confidence if there is any sign of BGRS in the GW signals.

The most notable finding of our study is that the required improvement is strongly dependent on the population model of the GW sources. If MBHBs obey the Q3d population model, then no more than a 4 order of magnitude improvement in $(S_a^{1/2}, S_x^{1/2})$ will be needed for all three detectors, even for the most demanding iEMRI signals. In fact, in this case the current design of μ Ares already has a very good ability to detect displacement memory, as is obvious from Table III. If, instead, MBHBs obey the pop III population model, then to detect the iEMRI signals, about (4, 7), (7, 8) and (7, 9) orders of magnitude improvement in $(S_a^{1/2}, S_x^{1/2})$ will be needed for TianQin, LISA and μ Ares, respectively. In this case, μ Ares will need about 2 orders of magnitude improvement in $(S_a^{1/2}, S_x^{1/2})$ to detect displacement memory.

It is also notable that, in the most demanding detection scenarios (those involving iEMRI or pop III), the required improvements in $S_a^{1/2}$ and $S_x^{1/2}$ can go up to 4–9 orders of magnitude. With such a level of technological improvement, environmental disturbances and strong coexisting GW signals can also become an obstacle. For example, a space magnetic field can cause an acceleration noise of the order $(S_a^{\text{Mag}})^{1/2} \sim 10^{-17} \text{ m/s}^2/\text{Hz}^{1/2}$ at around 10^{-3} Hz for inertial references [101, 102], and a rough estimate shows that for a full MBHB signal, an iEMRI signal will only cause a mismatch in roughly the order 10^{-11} . Both problems appear to be very difficult to overcome. As such, a significant challenge for future development can be expected if one needs to use the most demanding detection scenario to search for a BGRS.

ACKNOWLEDGMENTS

The work has been supported in part by the National Key Research and Development Program of China (Grant No. 2023YFC2206700), and the Fundamental Research Funds for the Central Universities, Sun Yat-sen University.

- [1] B. P. Abbott *et al.* (Virgo, LIGO Scientific), *Phys. Rev. Lett.* **116**, 061102 (2016), [arXiv:1602.03837 \[gr-qc\]](#).
- [2] J. R. Gair, M. Vallisneri, S. L. Larson, and J. G. Baker, *Living Rev. Rel.* **16**, 7 (2013), [arXiv:1212.5575 \[gr-qc\]](#).
- [3] N. Yunes and X. Siemens, *Living Rev. Rel.* **16**, 9 (2013), [arXiv:1304.3473 \[gr-qc\]](#).
- [4] E. Berti *et al.*, *Class. Quant. Grav.* **32**, 243001 (2015), [arXiv:1501.07274 \[gr-qc\]](#).
- [5] K. Yagi and L. C. Stein, *Class. Quant. Grav.* **33**, 054001 (2016), [arXiv:1602.02413 \[gr-qc\]](#).
- [6] L. Barack *et al.*, *Class. Quant. Grav.* **36**, 143001 (2019), [arXiv:1806.05195 \[gr-qc\]](#).
- [7] V. Cardoso and P. Pani, *Living Rev. Rel.* **22**, 4 (2019), [arXiv:1904.05363 \[gr-qc\]](#).
- [8] E. Barausse *et al.*, *Gen. Rel. Grav.* **52**, 81 (2020), [arXiv:2001.09793 \[gr-qc\]](#).
- [9] K. G. Arun *et al.* (LISA), *Living Rev. Rel.* **25**, 4 (2022), [arXiv:2205.01597 \[gr-qc\]](#).
- [10] J. Luo *et al.*, (2025), [arXiv:2502.20138 \[gr-qc\]](#).
- [11] E. Berti *et al.*, (2025), [arXiv:2505.23895 \[gr-qc\]](#).
- [12] B. P. Abbott *et al.* (LIGO Scientific, Virgo), *Phys. Rev. Lett.* **116**, 221101 (2016), [Erratum: *Phys. Rev. Lett.* **121**, 129902 (2018)], [arXiv:1602.03841 \[gr-qc\]](#).
- [13] B. P. Abbott *et al.* (LIGO Scientific, Virgo), *Phys. Rev. D* **100**, 104036 (2019), [arXiv:1903.04467 \[gr-qc\]](#).
- [14] R. Abbott *et al.* (LIGO Scientific, Virgo), *Phys. Rev. D* **103**, 122002 (2021), [arXiv:2010.14529 \[gr-qc\]](#).
- [15] R. Abbott *et al.* (LIGO Scientific, VIRGO, KAGRA), (2021), [arXiv:2112.06861 \[gr-qc\]](#).
- [16] A. G. Abac *et al.* (KAGRA, Virgo, LIGO Scientific), *Phys. Rev. Lett.* **135**, 111403 (2025), [arXiv:2509.08054 \[gr-qc\]](#).
- [17] A. G. Abac *et al.* (LIGO Scientific, VIRGO, KAGRA), (2025), [arXiv:2509.08099 \[gr-qc\]](#).
- [18] J. Mei, *Eur. Phys. J. Plus* **137**, 578 (2022).
- [19] J. Mei, *Eur. Phys. J. C* **83**, 16 (2023), [arXiv:2210.05434 \[gr-qc\]](#).
- [20] E. Barausse, *Mon. Not. Roy. Astron. Soc.* **423**, 2533 (2012), [arXiv:1201.5888 \[astro-ph.CO\]](#).
- [21] A. Klein *et al.*, *Phys. Rev. D* **93**, 024003 (2016), [arXiv:1511.05581 \[gr-qc\]](#).
- [22] J. Luo *et al.* (TianQin), *Class. Quant. Grav.* **33**, 035010 (2016), [arXiv:1512.02076 \[astro-ph.IM\]](#).
- [23] J. Mei *et al.* (TianQin), *PTEP* **2021**, 05A107 (2021), [arXiv:2008.10332 \[gr-qc\]](#).
- [24] J. Luo *et al.*, *Class. Quant. Grav.* **42**, 173001 (2025), [arXiv:2502.11328 \[gr-qc\]](#).
- [25] M. Colpi *et al.* (LISA), (2024), [arXiv:2402.07571 \[astro-ph.CO\]](#).
- [26] A. Sesana *et al.*, *Exper. Astron.* **51**, 1333 (2021), [arXiv:1908.11391 \[astro-ph.IM\]](#).
- [27] Z. Luo, Y. Wang, Y. Wu, W. Hu, and G. Jin, *PTEP* **2021**, 05A108 (2021).
- [28] K. Komori (DECIGO), (2025), [10.1142/s021827182540005x](#).
- [29] E. Berti, V. Cardoso, and A. O. Starinets, *Class. Quant. Grav.* **26**, 163001 (2009), [arXiv:0905.2975 \[gr-qc\]](#).
- [30] M. Campanelli and C. O. Lousto, *Phys. Rev. D* **59**, 124022 (1999), [arXiv:gr-qc/9811019](#).
- [31] K. Ioka and H. Nakano, *Physical Review D* **76**, 061503 (2007).
- [32] H. Nakano and K. Ioka, *Physical Review D* **76**, 084007 (2007).
- [33] L. London, D. Shoemaker, and J. Healy, *Physical Review D* **90**, 124032 (2014).
- [34] K. Mitman *et al.*, *Phys. Rev. Lett.* **130**, 081402 (2023), [arXiv:2208.07380 \[gr-qc\]](#).
- [35] M. H.-Y. Cheung *et al.*, *Phys. Rev. Lett.* **130**, 081401 (2023), [arXiv:2208.07374 \[gr-qc\]](#).
- [36] S. Ma and H. Yang, *Phys. Rev. D* **109**, 104070 (2024), [arXiv:2401.15516 \[gr-qc\]](#).
- [37] N. Khera, S. Ma, and H. Yang, *Phys. Rev. Lett.* **134**, 211404 (2025), [arXiv:2410.14529 \[gr-qc\]](#).
- [38] J. Redondo-Yuste, G. Carullo, J. L. Ripley, E. Berti, and V. Cardoso, *Phys. Rev. D* **109**, L101503 (2024), [arXiv:2308.14796 \[gr-qc\]](#).
- [39] H. Zhu *et al.*, *Phys. Rev. D* **109**, 104050 (2024), [arXiv:2401.00805 \[gr-qc\]](#).
- [40] A. G. Abac *et al.* (LIGO Scientific, Virgo, KAGRA), *Phys. Rev. Lett.* **135**, 111403 (2025), [arXiv:2509.08054 \[gr-qc\]](#).
- [41] A. G. Abac *et al.* (LIGO Scientific, Virgo, KAGRA), *Phys. Rev. Lett.* **136**, 041403 (2026), [arXiv:2509.08099 \[gr-qc\]](#).
- [42] Y. Yang, C. Shi, and Y.-M. Hu, (2025), [arXiv:2510.16903 \[gr-qc\]](#).
- [43] Y.-F. Wang, S. Ma, N. Khera, and H. Yang, (2026), [arXiv:2601.05734 \[gr-qc\]](#).
- [44] C. Shi, Q. Zhang, and J. Mei, *Phys. Rev. D* **110**, 124007 (2024), [arXiv:2407.13110 \[gr-qc\]](#).
- [45] Y. B. Zel'dovich and A. G. Polnarev, *Sov. Astron.* **18**, 17 (1974).
- [46] D. Christodoulou, *Phys. Rev. Lett.* **67**, 1486 (1991).
- [47] L. Blanchet and T. Damour, *Phys. Rev. D* **46**, 4304 (1992).
- [48] A. Strominger and A. Zhiboedov, *JHEP* **01**, 086 (2016), [arXiv:1411.5745 \[hep-th\]](#).
- [49] S. Pasterski, A. Strominger, and A. Zhiboedov, *JHEP* **12**, 053 (2016), [arXiv:1502.06120 \[hep-th\]](#).
- [50] D. A. Nichols, *Phys. Rev. D* **98**, 064032 (2018), [arXiv:1807.08767 \[gr-qc\]](#).
- [51] G. Compère, R. Oliveri, and A. Seraj, *JHEP* **10**, 116 (2020), [arXiv:1912.03164 \[gr-qc\]](#).
- [52] S. Weinberg, *Phys. Rev.* **140**, B516 (1965).
- [53] A. Strominger, *Lectures on the Infrared Structure of Gravity and Gauge Theory* (2017) [arXiv:1703.05448 \[hep-th\]](#).
- [54] A. Seraj, *JHEP* **05**, 283 (2021), [arXiv:2103.12185 \[hep-th\]](#).
- [55] S. Tahura, D. A. Nichols, and K. Yagi, *Phys. Rev. D* **104**, 104010 (2021), [arXiv:2107.02208 \[gr-qc\]](#).
- [56] S. M. Du and A. Nishizawa, *Phys. Rev. D* **94**, 104063 (2016), [arXiv:1609.09825 \[gr-qc\]](#).
- [57] S. Hou, T. Zhu, and Z.-H. Zhu, *Phys. Rev. D* **105**, 024025 (2022), [arXiv:2109.04238 \[gr-qc\]](#).
- [58] S. Hou, T. Zhu, and Z.-H. Zhu, *JCAP* **04**, 032 (2022), [arXiv:2112.13049 \[gr-qc\]](#).
- [59] S. Hou, A. Wang, and Z.-H. Zhu, *Phys. Rev. D* **109**, 044025 (2024), [arXiv:2309.01165 \[gr-qc\]](#).
- [60] A. Ashtekar, T. De Lorenzo, and N. Khera, *Gen. Rel. Grav.* **52**, 107 (2020), [arXiv:1906.00913 \[gr-qc\]](#).

- [61] S. Sun, C. Shi, J.-d. Zhang, and J. Mei, *Phys. Rev. D* **107**, 044023 (2023), arXiv:2207.13009 [gr-qc].
- [62] B. Goncharov, L. Donnay, and J. Harms, *Phys. Rev. Lett.* **132**, 241401 (2024), arXiv:2310.10718 [gr-qc].
- [63] V. B. Braginsky and K. S. Thorne, *Nature* **327**, 123 (1987).
- [64] P. D. Lasky, E. Thrane, Y. Levin, J. Blackman, and Y. Chen, *Phys. Rev. Lett.* **117**, 061102 (2016), arXiv:1605.01415 [astro-ph.HE].
- [65] M. Hübner, C. Talbot, P. D. Lasky, and E. Thrane, *Phys. Rev. D* **101**, 023011 (2020), arXiv:1911.12496 [astro-ph.HE].
- [66] M. Hübner, P. Lasky, and E. Thrane, *Phys. Rev. D* **104**, 023004 (2021), arXiv:2105.02879 [gr-qc].
- [67] S. Y. Cheung, P. D. Lasky, and E. Thrane, *Class. Quant. Grav.* **41**, 115010 (2024), arXiv:2404.11919 [gr-qc].
- [68] B. P. Abbott *et al.* (LIGO Scientific), *Class. Quant. Grav.* **34**, 044001 (2017), arXiv:1607.08697 [astro-ph.IM].
- [69] M. Punturo *et al.*, *Class. Quant. Grav.* **27**, 194002 (2010).
- [70] S. Sun, C. Shi, J.-d. Zhang, and J. Mei, *Phys. Rev. D* **110**, 024050 (2024), arXiv:2401.11416 [gr-qc].
- [71] K. Islo, J. Simon, S. Burke-Spolaor, and X. Siemens, (2019), arXiv:1906.11936 [astro-ph.HE].
- [72] H. Inchauspé, S. Gasparotto, D. Blas, L. Heisenberg, J. Zosso, and S. Tiwari, *Phys. Rev. D* **111**, 044044 (2025), arXiv:2406.09228 [gr-qc].
- [73] N. Seto, *Mon. Not. Roy. Astron. Soc.* **400**, L38 (2009), arXiv:0909.1379 [astro-ph.CO].
- [74] R. van Haasteren and Y. Levin, *Mon. Not. Roy. Astron. Soc.* **401**, 2372 (2010), arXiv:0909.0954 [astro-ph.IM].
- [75] M. S. Pshirkov, D. Baskaran, and K. A. Postnov, *Mon. Not. Roy. Astron. Soc.* **402**, 417 (2010), arXiv:0909.0742 [astro-ph.CO].
- [76] J. M. Cordes and F. A. Jenet, *Astrophys. J.* **752**, 54 (2012).
- [77] D. R. Madison, J. M. Cordes, and S. Chatterjee, *Astrophys. J.* **788**, 141 (2014), arXiv:1404.5682 [astro-ph.HE].
- [78] Z. Arzumanyan *et al.* (NANOGrav), *Astrophys. J.* **810**, 150 (2015), arXiv:1501.05343 [astro-ph.GA].
- [79] G. Agazie *et al.* (NANOGrav), *Astrophys. J.* **963**, 61 (2024), arXiv:2307.13797 [gr-qc].
- [80] C. Barcelo, M. Visser, and S. Liberati, *Int. J. Mod. Phys. D* **10**, 799 (2001), arXiv:gr-qc/0106002.
- [81] C. Barcelo, S. Liberati, and M. Visser, *Living Rev. Rel.* **8**, 12 (2005), arXiv:gr-qc/0505065.
- [82] B. L. Hu, *J. Phys. Conf. Ser.* **174**, 012015 (2009), arXiv:0903.0878 [gr-qc].
- [83] L. Sindoni, *SIGMA* **8**, 027 (2012), arXiv:1110.0686 [gr-qc].
- [84] S. Carlip, *Stud. Hist. Phil. Sci. B* **46**, 200 (2014), arXiv:1207.2504 [gr-qc].
- [85] N. S. Linnemann and M. R. Visser, *Stud. Hist. Phil. Sci. B* **64**, 1 (2018), arXiv:1711.10503 [physics.hist-ph].
- [86] M. Isi, W. M. Farr, M. Giesler, M. A. Scheel, and S. A. Teukolsky, *Phys. Rev. Lett.* **127**, 011103 (2021), arXiv:2012.04486 [gr-qc].
- [87] U. Sperhake, V. Cardoso, F. Pretorius, E. Berti, and J. A. Gonzalez, *Phys. Rev. Lett.* **101**, 161101 (2008), arXiv:0806.1738 [gr-qc].
- [88] U. Sperhake, V. Cardoso, F. Pretorius, E. Berti, T. Hinderer, and N. Yunes, *Phys. Rev. Lett.* **103**, 131102 (2009), arXiv:0907.1252 [gr-qc].
- [89] U. Sperhake, E. Berti, V. Cardoso, and F. Pretorius, *Phys. Rev. Lett.* **111**, 041101 (2013), arXiv:1211.6114 [gr-qc].
- [90] J. Healy, I. Ruchlin, C. O. Lousto, and Y. Zlochower, *Phys. Rev. D* **94**, 104020 (2016), arXiv:1506.06153 [gr-qc].
- [91] G. Bozzola, *Phys. Rev. Lett.* **128**, 071101 (2022), arXiv:2202.05310 [gr-qc].
- [92] J. Healy and C. O. Lousto, *Phys. Rev. Lett.* **131**, 071401 (2023), arXiv:2301.00018 [gr-qc].
- [93] J. Healy, A. Ciarfella, and C. O. Lousto, (2024), arXiv:2410.20239 [gr-qc].
- [94] Y. Fang, C. Shi, and J. Mei, (2025), arXiv:2512.04851 [gr-qc].
- [95] T. Robson, N. J. Cornish, and C. Liu, *Class. Quant. Grav.* **36**, 105011 (2019), arXiv:1803.01944 [astro-ph.HE].
- [96] C. García-Quirós, M. Colleoni, S. Husa, H. Estellés, G. Pratten, A. Ramos-Buades, M. Mateu-Lucena, and R. Jaume, *Phys. Rev. D* **102**, 064002 (2020), arXiv:2001.10914 [gr-qc].
- [97] G. Pratten, S. Husa, C. Garcia-Quiros, M. Colleoni, A. Ramos-Buades, H. Estelles, and R. Jaume, *Phys. Rev. D* **102**, 064001 (2020), arXiv:2001.11412 [gr-qc].
- [98] M. Colleoni, M. Mateu-Lucena, H. Estellés, C. García-Quirós, D. Keitel, G. Pratten, A. Ramos-Buades, and S. Husa, *Phys. Rev. D* **103**, 024029 (2021), arXiv:2010.05830 [gr-qc].
- [99] J. Valencia, R. Tenorio, M. Rosselló-Sastre, and S. Husa, *Phys. Rev. D* **110**, 124026 (2024), arXiv:2406.16636 [gr-qc].
- [100] E.ourgoulhon, A. Le Tiec, F. H. Vincent, and N. Warburton, *Astron. Astrophys.* **627**, A92 (2019), arXiv:1903.02049 [gr-qc].
- [101] P. Jia-Hui, Z. Ji-Xiang, W. Hong, S. Wei, N. Yi-Wei, G. Jin-Han, and Z. Rui-Sheng, *Sci. Rep.* **15**, 23287 (2025), arXiv:2502.10142 [physics.space-ph].
- [102] W. Su, *Rev. Mod. Plasma Phys.* **9**, 26 (2025), arXiv:2509.16982 [astro-ph.SR].

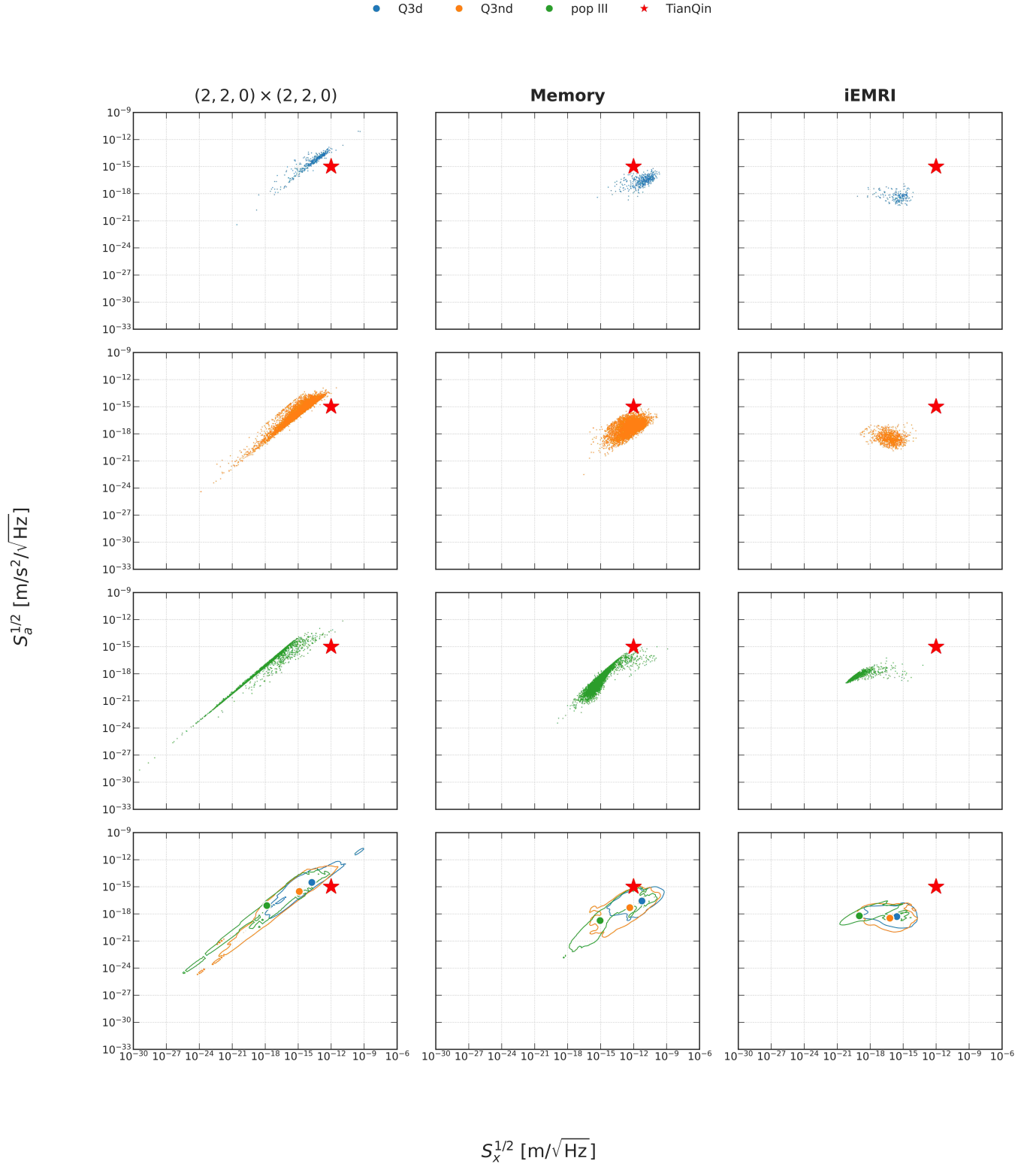


FIG. 4. Distribution of optimal values of $(S_a^{1/2}, S_x^{1/2})$ for TianQin. The last row compares the major distribution regions and their centers for different population models. See main text for more explanation.

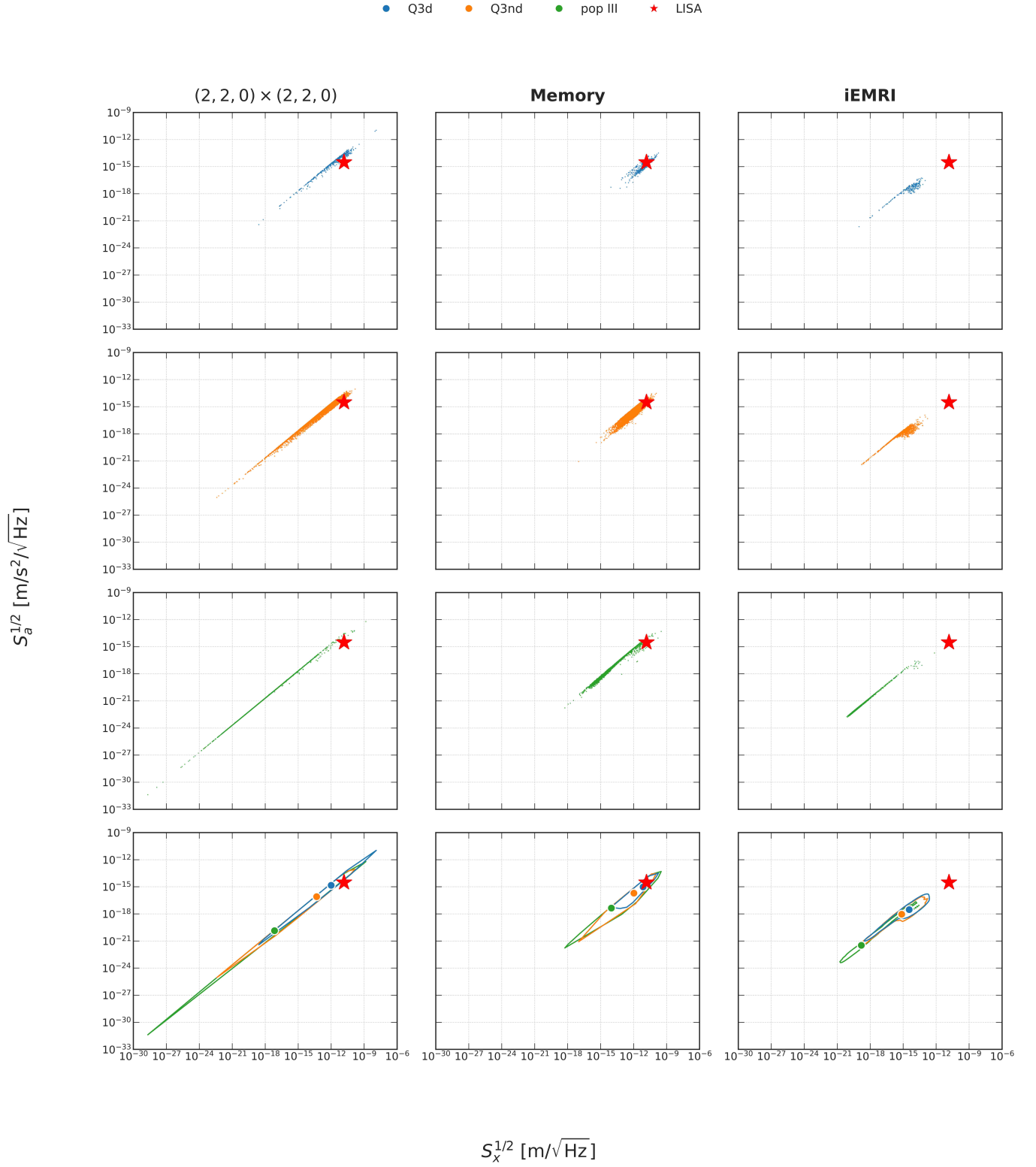


FIG. 5. Distribution of optimal values of $(S_a^{1/2}, S_x^{1/2})$ for LISA. The last row compares the major distribution regions and their centers for different population models. See main text for more explanation.

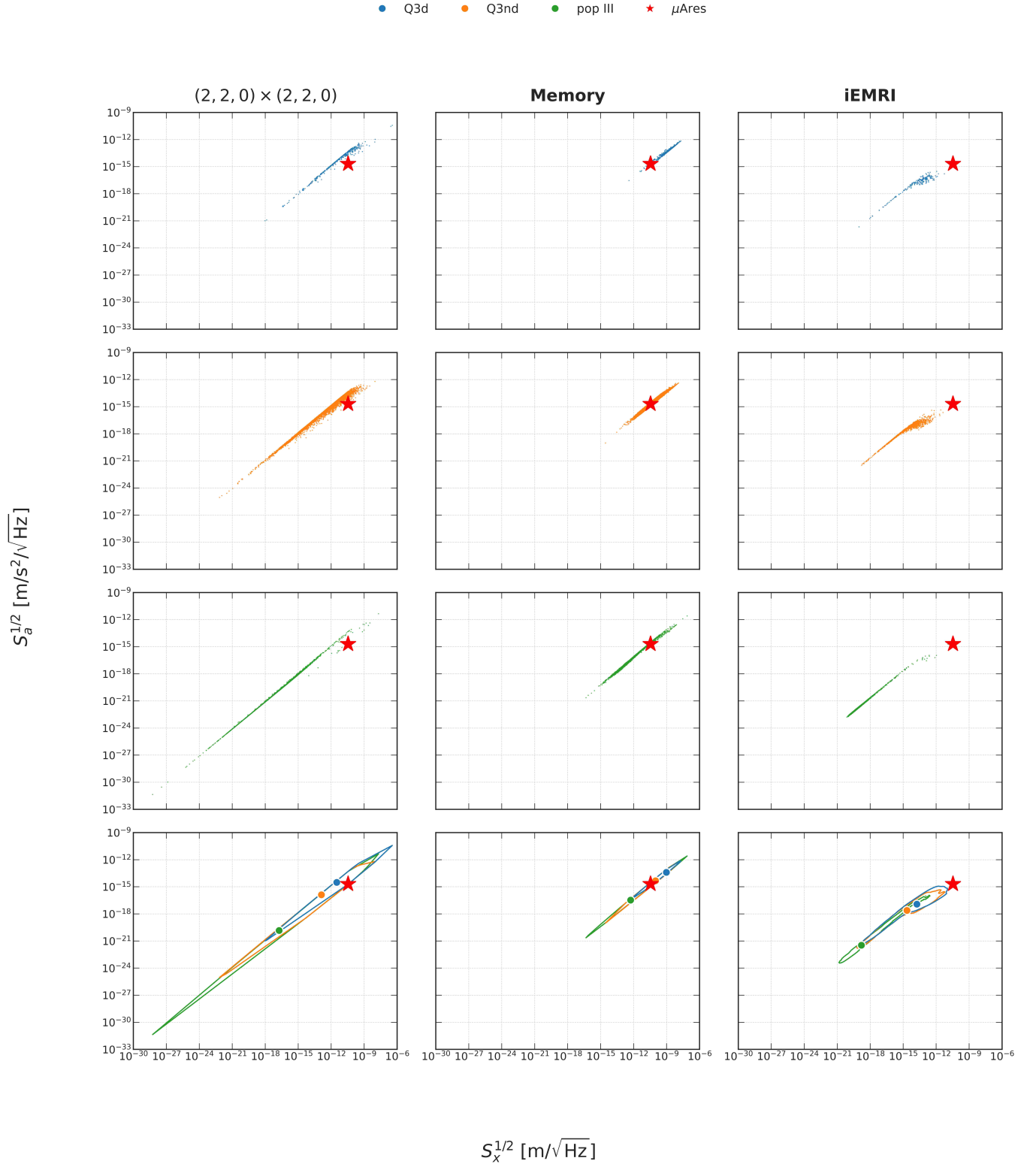


FIG. 6. Distribution of optimal values of $(S_a^{1/2}, S_x^{1/2})$ for μ Ares. The last row compares the major distribution regions and their centers for different population models. See main text for more explanation.